frontiers | Frontiers in Marine Science

TYPE Original Research
PUBLISHED 25 November 2022
DOI 10.3389/fmars.2022.1059746

OPEN ACCESS

EDITED BY
Elinor Andrén,
Södertörn University, Sweden

REVIEWED BY
Irina Polovodova Asteman,
University of Gothenburg, Sweden
Shiyong Yu,
Jiangsu Normal University, China

*CORRESPONDENCE
Zhanghua Wang
zhwang@geo.ecnu.edu.cn

SPECIALTY SECTION
This article was submitted to Coastal Ocean Processes, a section of the journal Frontiers in Marine Science

RECEIVED 02 October 2022
ACCEPTED 31 October 2022
PUBLISHED 25 November 2022

CITATION
Lyu Y, Xu H, Meadows ME and Wang Z (2022) Early to mid-Holocene sedimentary environmental evolution in the palaeo-Ningbo Bay, East China and its implications for Neolithic coastal settlement.
Front. Mar. Sci. 9:1059746.
doi: 10.3389/fmars.2022.1059746

Early to mid-Holocene sedimentary environmental evolution in the palaeo-Ningbo Bay, East China and its implications for Neolithic coastal settlement

Ye Lyu[1], Hao Xu[2], Michael E. Meadows[3,4,5] and Zhanghua Wang[1,6,7]*

[1]State Key Laboratory of Estuarine and Coastal Research, East China Normal University, Shanghai, China, [2]Department of Geography and Spatial Information Techniques, Ningbo University, Ningbo, China, [3]Department of Environmental and Geographical Science, University of Cape Town, Rondebosch, South Africa, [4]School of Geographic Sciences, East China Normal University, Shanghai, China, [5]College of Geography and Environmental Sciences, Zhejiang Normal University, Jinhua, China, [6]Institute of Archaeological Science, Fudan University, Shanghai, China, [7]Southern Marine Science and Engineering Guangdong Laboratory, Zhuhai, China

The Ningbo Plain on the East China coast is an important center of Neolithic culture, and associated settlements were influenced by changing sea levels and the geomorphological and hydrological environments of the palaeo-Ningbo Bay, the details of which are still subject to debate. This study is based on two well-dated sediment cores obtained from the Ningbo Plain, and here we report analyses of their sedimentology and foraminifera to reveal the infilling history of the palaeo-Ningbo Bay and its association with Neolithic occupation. The lithology of the largely muddy sediments and the dominance of euryhaline and brackish water foraminiferal species are indicative of an intertidal to a subtidal environment in the palaeo-bay during the early to mid-Holocene. Abrupt coarsening of sediment grain size and a corresponding increase in the abundance of foraminiferal species of inner and middle shelf environments occurred at ca. 8.8 cal. kyr BP and 7.6 cal. kyr BP, reflecting two major events of strengthened marine transgression that correspond to the rapid global sea-level rise events of Meltwater pulses (MWPs) 1C and 1D, respectively. A marked increase in the relative abundance of *Ammonia annectens* and *Ammonia compressiuscula* during ca. 7.5–7.1 cal. kyr BP further indicates frequent storm surges at that time. Between the two rapid transgression events, aggradation of tidal flats prevailed after ca. 8.0 cal. kyr BP, which provided a suitable setting for Neolithic settlements, as indicated by the recently discovered Jingtoushan site. However, the transgression

sequence associated with the latter, the MWP-1D event, caused a regional cultural interruption at ca. 7.6 cal. kyr BP. Infilling and coastal marsh development in the palaeo-Ningbo Bay occurred progressively after ca. 7.0 cal. kyr BP and are associated with the emergence of the Hemudu culture.

KEYWORDS

Foraminifera, grain size, tidal flat, sea-level change, MWP-1C, MWP-1D, storm surge

Highlights

1. The Ningbo Plain was fully inundated to form an embayment at ca. 9,600 years ago.
2. Two events of accelerated transgression occurred at 8.8 and 7.6 cal. kyr BP.
3. Tidal flats developed at ca. 8.0 cal. kyr BP in response to stable sea levels.
4. Neolithic settlement on the coastal lowlands is closely linked to sea level changes.

1 Introduction

Coastal plains are located at the land–sea transition and are characterized by fragile ecological environments that are highly sensitive to sea-level change (Benassai et al., 2015; Wang et al., 2017). Sea-level rise intensifies natural disasters such as seawater intrusion, coastal flooding, and accelerated erosion, all of which seriously constrain sustainable development in the coastal plain (Woodruff et al., 2013; Wang et al., 2017; IPCC, 2019). The history of Holocene sea-level change and the accompanying sedimentary evolution has had a remarkable impact on the rise and fall of Neolithic occupation in coastal zones and has become an important focus of research (e.g., Zong et al., 2007; Innes et al., 2009; Wang et al., 2012; Wang et al., 2018; He et al., 2020a).

The Ningbo Plain, on the southeast coast of Hangzhou Bay, East China, is typical of coastal lowlands that lie downdrift of major rivers, in this case the Yangtze (Figure 1A). Previous palaeoenvironmental studies and documented historical records of extreme events indicate that sea-level rise and associated saltwater intrusions are significant natural hazards both in the past and present (Innes et al., 2009; Wang et al., 2018; Tang, 2020). This plain is well known to have been an important center for Neolithic settlements, and several sites have already been excavated (Zheng et al., 2012; Wang et al., 2018; Tang et al., 2019; Huang et al., 2020; He et al., 2020a; Huang et al., 2021). A recently discovered Neolithic site (Jingtoushan; Figure 1B) comprising shell mounds buried by ca. 5–11 m of marine sediments and formed about 8,000 years ago (Sun et al., 2021) is to date the earliest known Neolithic site on the Ningbo Plain. This important archaeological discovery highlights the need to reconstruct the associated early to mid-Holocene evolutional history of the Ningbo Plain in order to reveal factors controlling the temporal and spatial pattern of its Neolithic occupation.

Previous studies have suggested a stepwise rise in early to middle Holocene sea levels (Liu et al., 2004; Bird et al., 2007). Particularly, two events of rapid sea-level rise have been widely reported: the first was the Meltwater Pulse (MWP) associated with the outburst of proglacial Lake Agassi-Ojibway at ca. 8.5 cal. kyr BP, which has been claimed as a global event (Hijma and Cohen, 2010; Harrison et al., 2019); the second event at ca. 7.6 cal. kyr BP was first reported from the Caribbean coral records and termed as a catastrophic rise event (CRE-3) by Blanchon and Shaw (1995). Bird et al. (2010) further suggested that the relatively stable sea levels during these two events had precipitated coastal sedentary agriculture such as the rice cultivation of the Neolithic Kuahuqiao Culture in East China. However, there is still debate about the magnitude and timing of the two events. Harrison et al. (2019) reviewed all publications on the late Quaternary events of rapid sea-level rise and proposed that most previously reported rapid sea-level rises during the early Holocene are likely to be local events except the one associated with the MWP induced by the drainage of Lake Agassiz-Ojibway.

Studies of Holocene relative sea-level changes on the East China coast are limited, and only a few provide clear evidence of accelerated Holocene sea-level rise in the early to middle Holocene. For example, Wang et al. (2012) and Wang et al. (2013) document a ca. 10 mm/yr rate of increase during 7.4–7.2 cal. kyr BP and ca. 30 mm/yr during 8.5–8.3 cal. kyr BP, respectively, while Xiong et al. (2020) suggest a rapid rise at ca. 7.5 cal. kyr BP. In addition, as evidenced by an increase in saltmarsh herb pollen and salt-tolerant diatoms, the Neolithic site of Kuahuqiao, on the southwest coast of Hangzhou Bay (Figure 1A), was inundated by seawater at ca. 7,550 cal. yr BP, which resulted in the termination of rice cultivation there (Zong et al., 2007). However, others have argued that it was the

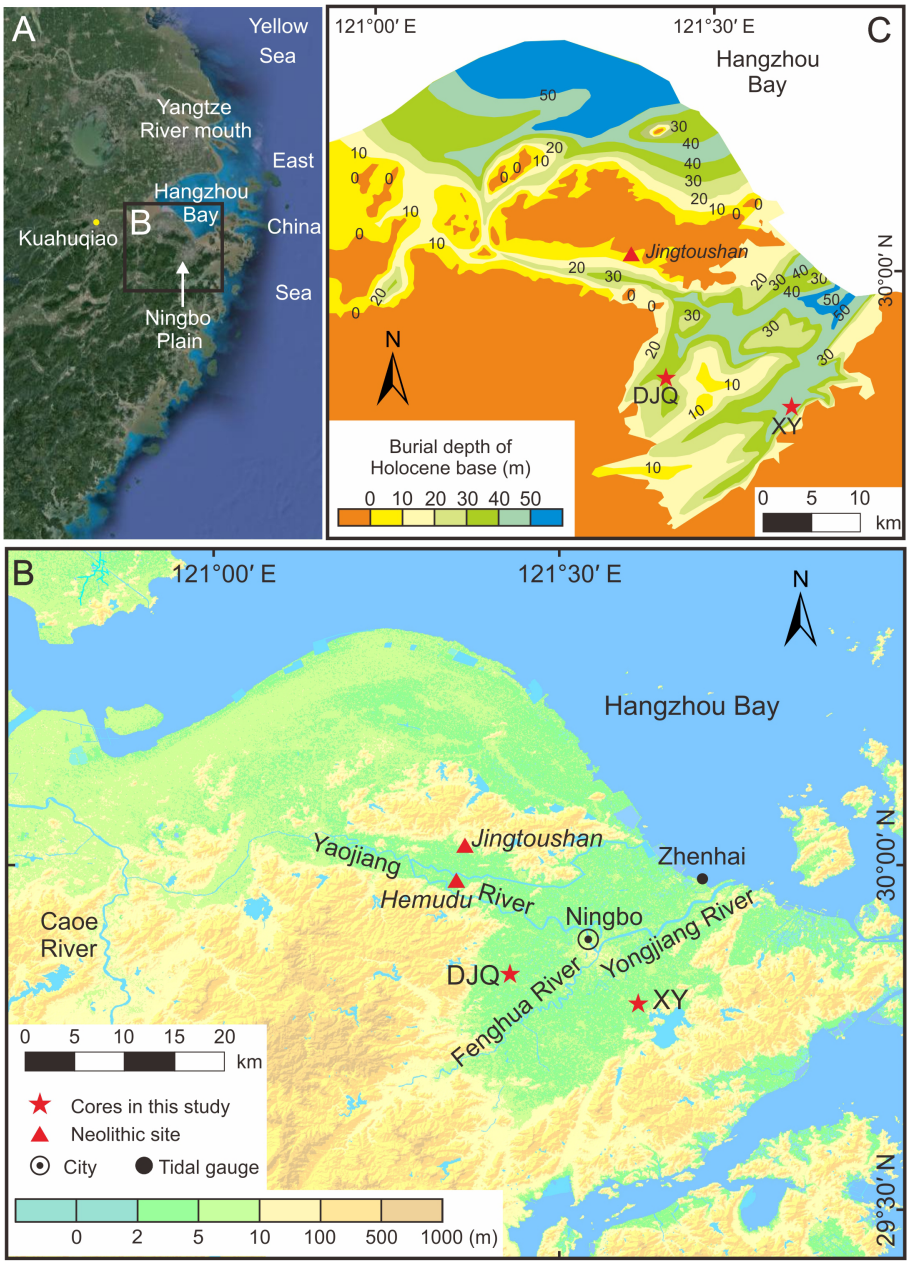

FIGURE 1
Location of **(A)** the study area and the Kuahuqiao site and **(B)** the Neolithic Jingtoushan and Hemudu sites and sediment cores. **(C)** Buried depth of the Holocene base, which is identified from the stiff mud of palaeosol and river channel gravelly sand formed during the late Pleistocene (after Xu, 1987; Yan, 1987).

stabilization of relative sea levels after 7.6 cal. kyr BP that was key to sustained Neolithic occupation on the coast of Hangzhou Bay (cf. Liu et al., 2018; Liu et al., 2020). Accordingly, additional, well-dated, multi-proxy sedimentary records are needed to resolve environmental evolution and associated sea level changes along the East China coast, along with their implications for Neolithic cultures.

In this study, we obtained two sediment cores in the Ningbo Plain on the southeast coast of Hangzhou Bay, East China (Figure 1B) and provided AMS ^{14}C ages, lithology, grain size, and foraminiferal evidence to reveal details of relative sea-level changes and their impacts on the sedimentary evolution of palaeo-Ningbo Bay and to investigate the relationship between Neolithic settlement and environmental changes in the bay.

2 Environmental setting

The Ningbo Plain (121°21'E–121°51'E, 29°38'N–30°10'N) is located on the southeast coast of Hangzhou Bay, East China. It is surrounded by uplands in the east, south, and west and is open to Hangzhou Bay in the north (Figure 1B). The low-lying plain has a mean elevation of ca. 2.2 m (Ningbo Water Conservation Annals Compilation Committee, 2006). The underlying bedrock is mostly buried 30–60 m deep mainly by Holocene sediments (Sun, 2013). During the last glacial maximum (LGM), two palaeo-incised valleys extending southwest-northeast developed in the eastern and western parts of the plain, while terraces dominated the central part (Figure 1C; Yan, 1987).

A subtropical monsoon climate prevails in the study area, with a mean annual average temperature of 16.7°C and a mean annual precipitation of 1,400–1,500 mm (Ningbo Water Conservation Annals Compilation Committee, 2006; Huang et al., 2013). The coastal plain lies in the path of frequent northwest Pacific tropical cyclones, extreme events associated with strong winds, heavy rain, and storm surges (Huang et al., 2013). The uplands surrounding the Ningbo Plain yield a number of rivers, which converge into the Yongjiang River that flows northeast, with an annual discharge of 2.86×10^9 m^3 into Hangzhou Bay (Figure 1B; Ningbo Water Conservation Annals Compilation Committee, 2006). The combination of river floods and storm surges regularly results in widespread waterlogging on the plain (Huang et al., 2013). Irregular semi-diurnal tides occur on the coast with an average tidal range of 1.85 m at the Zhenhai gauge station (Figure 1B; Tang, 2020).

3 Materials and methods

In 2016, we obtained two sediment cores, XY (121°37'06"E, 29°48'15"N; recovery rate 99%) and DJQ (121°26'16"E, 29°51'19"E; recovery rate 95%), with a 9-cm-diameter rotary drill from the eastern and western parts, i.e., in the palaeo-incised valleys, of the Ningbo Plain (Figures 1B, C). Ground elevation, measured by a total station theodolite (GPT-100R, TOPCOM), was recorded as 1.7 m and 2.4 m (Yellow Sea Datum in 1985) at sites XY and DJQ, respectively. XY has a total length of 46.8 m, and DJQ is 41.2 m. After transport to the laboratory, the cores were split in half, immediately photographed, and described for lithology, including color, texture, and structure, macrofossils, and type of contact between lithological units.

In core XY, stiff muds are present between 46.8 and 46.48 m, overlain by a succession of gravelly sand at 46.48–44.19 m, which is characterized largely by subangular gravels (maximum size 5 cm × 2 cm × 2 cm). Muddy sediments prevail above 44.19 m. Gravelly sand occurs at a depth of 37–35.85 m at the base of the core DJQ. It is overlain by muddy sediments measuring 35.85 m thick. In this study, we only sampled and analyzed the muddy sediments above the gravelly base in both cores. We collected six samples of plant material (a horizontally lying stem or leaf of an herbaceous plant without the identification of species) and three samples of shell fragments from XY and five samples of plant material, two samples of organic-rich mud, and three samples of shell fragments from DJQ for AMS ^{14}C dating (Table 1). We washed and sieved the plant material and shell fragments through 250 mesh with distilled water and then dried the samples at 40°C. We then picked out the dating material under the microscope before sending it to Beta Analytic (US) for AMS ^{14}C dating. In the Beta Analytic, pretreatment with acid wash, acid/alkali/acid, and acid etch were performed for organic sediments, plant material, and shell samples, respectively, and the $\delta^{13}C$ values were measured separately in an isotope ratio mass spectrometer (IRMS) to help identify the taxa of the dating material. All AMS ^{14}C ages were calibrated using the Calib 8.20 program (Stuiver et al., 2022), and a marine reservoir value of $\triangle R = 71 \pm 31$ (Yoneda et al., 2007) was used only for shell samples because plant material and organic-rich mud are considered to be a terrestrial origin. The program "Clam 2.2" (Blaauw, 2010) was then employed to establish the age–depth models and obtain the weighted average age of each depth in two cores.

We further collected 130 samples (each 2 cm thick) from core XY at intervals of 10–50 cm for grain size and foraminiferal analyses. Core DJQ was not sampled for these same analyses as it was considered that these would be duplicates because we observed consistent sediment sequences between the two cores. Grain size analysis was performed using an LS13320 laser diffraction particle size analyzer (Beckman Coulter, US; measurement range 0.039–2000 μm) at the East China Normal University. Pretreatment included mixing to ensure uniformity and drying at 40°C. Each sediment sample of ca. 0.2 g was treated with 10% HCl and 10% H_2O_2 to remove carbonates and organic matter, respectively. After washing in distilled water and settling, 5% Calgon was added to ensure full dispersion in the ultrasonic bath before measurement. The percentages of clay, silt, and sand components were calculated after measurement.

Deposit samples for foraminiferal analysis were homogenized and dried at 40°C. Each sample was accurately weighed to 20 g and wet sieved through a 280-mesh (55 μm) screen based on previous experience that small foraminiferal tests are common in the muddy sediments of the study area (Wang et al., 1988). The microfossils were identified and counted under a binocular microscope (magnification ×50) following the taxonomic concepts of Wang et al. (1988). All foraminiferal tests in the 20 g dry samples were counted as absolute abundance (counts/20 g dry sample). Owing to the generally low absolute abundance in the study area, those samples with total counts exceeding 100 were used to calculate the relative abundance (i.e., percentage of the total counts) of each species (Wang et al., 1988). Those species exceeding 2% in at least five samples were used in the palaeo-environmental analysis.

TABLE 1 AMS ^{14}C ages and their calibrations for cores XY and DJQ.

Core	Depth (m)	Dating materials	^{14}C age (yr BP)	δ^{13}C (‰)	Calibrated age (cal. yr BP)			Laboratory number
					2 sigma	Prob.	Median	
XY	2.20	Plant	2,110 ± 30	−29.8	1,995–2,150	0.969	2,075	Beta515757
	3.52	Plant	5,290 ± 40	−26.6	5,990–6,190	0.920	6,080	Beta520172
	15.69	Shell	7,600 ± 30	−8.8	7,655–7,950	1.000	7,805	Beta515755
	16.53	Shell	7,510 ± 30	−2.3	7,565–7,870	1.000	7715	Beta520168
	19.49	Shell	7,960 ± 30	−2.7	8,015–8,335	1.000	8,180	Beta520169
	38.53	Plant	8,990 ± 30	−25.9	10,130–10,235	0.900	10,190	Beta520173
	39.36	Plant	9,220 ± 40	−26.7	10,250–10,500	1.000	10,380	Beta520170
	41.69	Plant	9,240 ± 40	−28.3	10,255–10,510	0.985	10,405	Beta520171
	42.99	Plant	9,500 ± 30	−27.5	10,655–11,070	1.000	10,760	Beta515754
DJQ	2.63	Organic-rich mud	4,680 ± 30	−26	5,320–5,475	1.000	5,395	Beta515753
	4.76	Organic-rich mud	5,980 ± 30	−25.4	6,735–6,900	0.992	6,820	Beta520178
	5.56	Plant	6,190 ± 30	−29.4	6,990–7,165	0.985	7,080	Beta520179
	11.45	Shell	7,090 ± 30	−4	7,175–7,470	1.000	7,330	Beta515752
	14.10	Shell	7,260 ± 30	−2	7,335–7,620	1.000	7,485	Beta520174
	16.74	Shell	7,360 ± 30	−1.1	7,425–7,710	1.000	7,575	Beta520175
	19.44	Plant	7,200 ± 30	−29.1	7,940–8,040	0.978	8,000	Beta520176
	27.78	Plant	7,600 ± 40	−27.9	8,340–8,455	0.982	8,400	Beta515751
	34.47	Plant	8,850 ± 30	−28.2	9,765–10,155	1.000	9,970	Beta520177
	35.56	Plant	8,850 ± 30	−11	9,765–10,155	1.000	9,970	Beta515750

4 Results

4.1 AMS^{14}C dating and age-depth model

4.1.1 Core XY

The nine AMS ^{14}C ages in the core XY are in the range of 10,760–2,075 cal. yr BP (median-probability value; Table 1). The plant samples have δ^{13}C values ranging from −29.8‰ to −25.9‰, indicating the origin of terrestrial C3 plants (Lamb et al., 2006). Shell samples have δ^{13}C values of −8.8 to −2.3‰, reflecting brackish water and marine species (McConnaughey and Gillilin, 2008). The calibrated ages generally increase with depth except for an age reversal at 15.69 m, which however, has an overlapped range with the age at 16.53 m (Table 1; Figure 2A). This reversed age was excluded from the age–depth modeling by the "Clam" program. Besides, there is a strong contrast in sedimentation rates between the periods before and after 6.0 cal. kyr BP, which indicates that sedimentation at the core site mainly occurred before 6.0 cal. kyr BP (Figure 2A).

4.1.2 Core DJQ

The ten radiocarbon ages span from 9,970 to 5,395 cal. yr BP (Table 1) and increase with depth. The δ^{13}C values of most samples of plant and organic-rich mud range between −29.4‰ and −25.4‰, reflecting the origin of terrestrial C3 plants; there is one plant sample at 35.56 m having a δ^{13}C value of −11‰, indicating the origin of a C4 plant (Lamb et al., 2006). The δ^{13}C values of shell samples vary from −4‰ to −1.1‰, indicating brackish water and marine species (McConnaughey and Gillilin, 2008). All ages were applied in the calculation of the age–depth model by "Clam" (Figure 2B). Rapid deposition occurred at the core site before 7.0 cal. kyr BP. In particular, remarkably high deposition rates occurred at 8.4–8.0 cal. kyr BP and 7.6–7.5 cal. kyr BP, reaching 21.3 mm/yr and 28.7 mm/yr, respectively (Figure 2B). The deposition rate obviously reduced after 7.0 cal. kyr BP and further reduced after ca. 5.4 cal. kyr BP.

4.2 Core lithology

4.2.1 Core XY

Based on lithological observations, including changes in color, texture, sediment type, and the presence of shell fragments in the sediment column, the muddy sedimentary sequence above 44.19 m has been divided into nine units (units I–IX) from bottom to top (Figure 3).

Unit I (44.19–41.92 m; 11,125–10,525 cal. yr BP) is composed of yellowish gray and dark gray clayey silt with some plant fragments (Figure 4A). The upper section has a high organic matter content. Some leaching structures are present in the lower section. Unit I exhibits gradual contact with the overlying unit II.

Unit II (41.92–36.20 m; 10,525–9,940 cal. yr BP) consists of gray homogeneous mud with clumps and laminations of silty

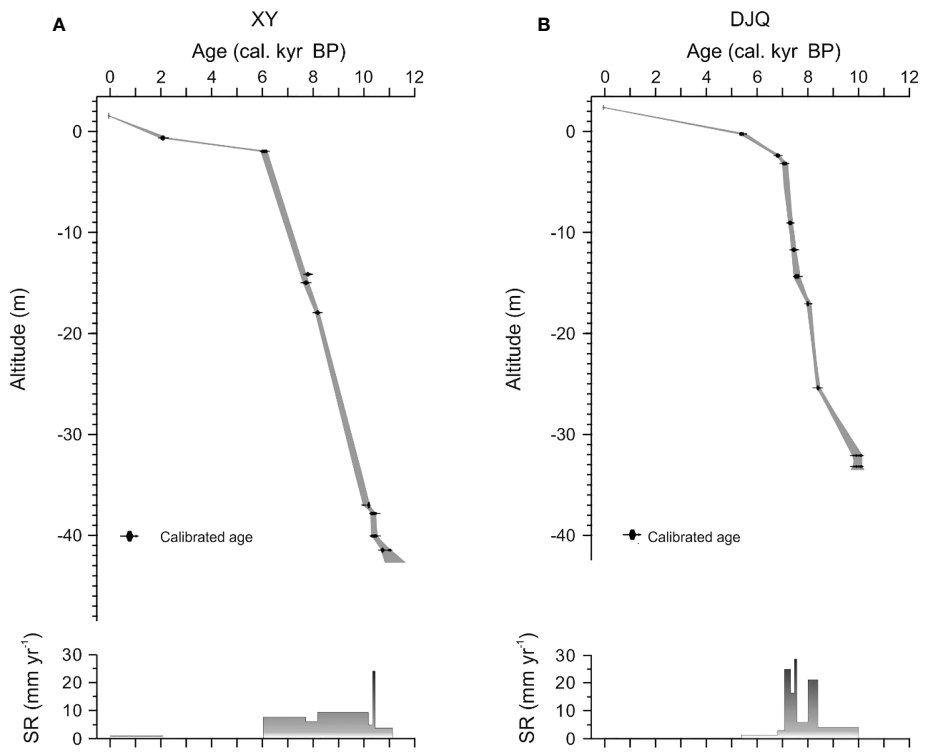

FIGURE 2
Age-depth models of cores XY **(A)** and DJQ **(B)**. The ages of the marine shell samples were inserted manually, as the Clam software does not facilitate the inclusion of terrestrial and marine samples in the model. Changes in sedimentation rate (SR) in each core are also indicated.

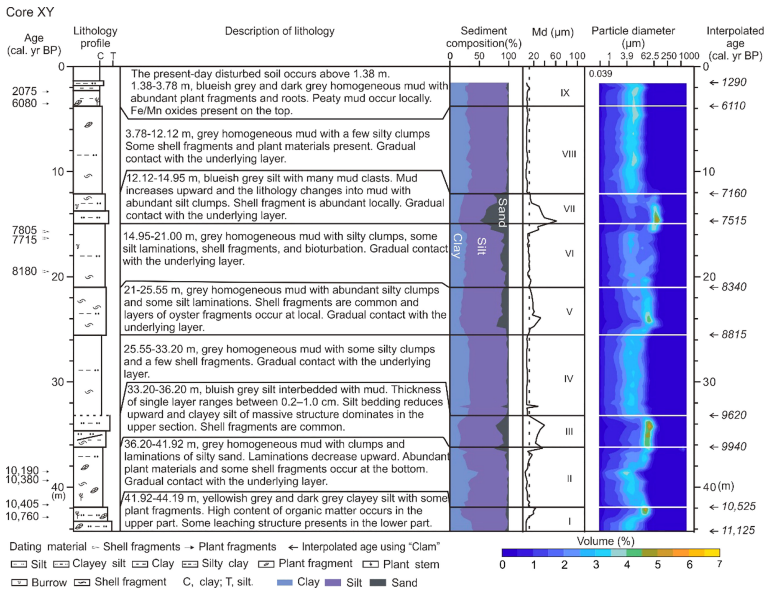

FIGURE 3
Sedimentary profile of core XY, including lithology description, calibrated radiocarbon ages, grain size composition, median grain size, and the distribution of volume frequency of grain size. Interpolated ages by "Clam" at the boundaries of each unit are also indicated on the right side.

sand (Figure 4B), which decrease upwards. Abundant plant remains and some shell fragments occur at the base. There is gradual contact with the overlying unit III.

Unit III (36.20–33.20 m; 9,940–9,620 cal. yr BP) comprises blueish-gray silt interbedded with mud, with layers ranging between 0.2 and 1.0 cm. Silt layers decline upwards, and the clayey silt of massive structures dominates the upper part (Figure 4C). Shell fragments are common, and some intact shells are locally present.

Unit IV (33.20–25.55 m; 9,620–8,815 cal. yr BP) is composed of gray homogeneous mud with occasional clumps of silt (Figure 4D) and a few shell fragments. There is gradual contact with the overlying unit V.

Unit V (25.55–21.00 m; 8,815–8,340 cal. yr BP) is dominated by gray homogeneous mud with abundant clumps of silt and some silt laminations (Figure 4E). Shell fragments are common, and locally there are layers dominated by oyster shell fragments. There is gradual contact with the overlying unit VI.

Unit VI (21.00–14.95 m; 8,340–7,515 cal. yr BP) also consists of gray homogeneous mud. Clumps of silt largely decrease, and silty laminations only occasionally occur (Figure 4F). Shell fragments and bioturbation are observed locally.

Unit VII (14.95–12.12 m; 7,515–7,160 cal. yr BP) is composed of blueish-gray silt with numerous mud clasts (Figure 4G). Mud content increases upwards, but there are abundant silt clumps in the upper part (Figure 4H). Shell fragments are locally abundant. There is gradual contact with the overlying unit VIII.

Unit VIII (12.12–3.78 m; 7,160–6,110 cal. yr BP) is composed of gray, homogeneous mud with a few silty clumps

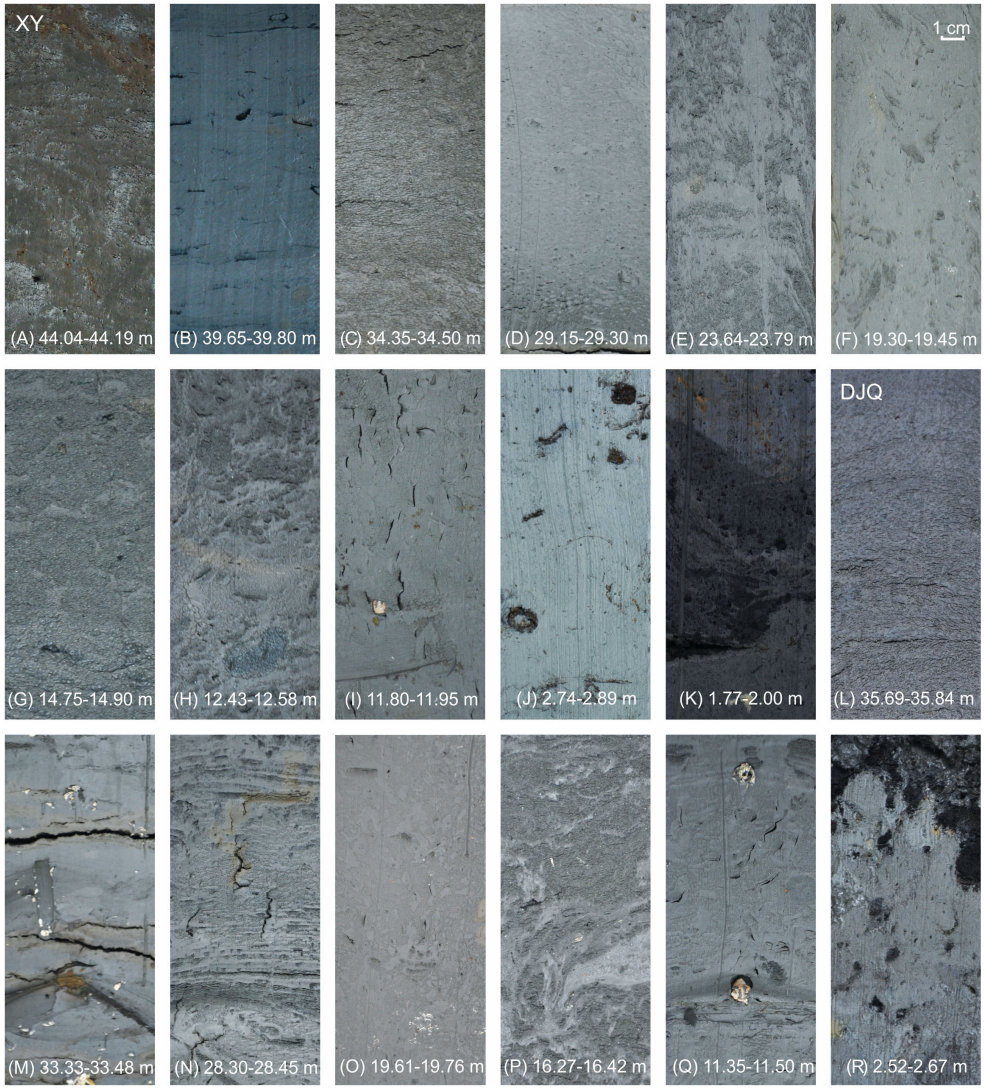

FIGURE 4
Photographs of typical lithological elements in cores XY **(A–K)** and DJQ **(L–R)**.

(Figure 4I). Some shell fragments and plant materials are present. There is gradual contact with the overlying unit IX.

Unit IX (3.78–1.38 m; 6,110–1,290 cal. yr BP) comprises blueish-gray and dark-gray homogeneous mud with abundant plant fragments and roots (Figures 4J, K). Peaty mud occurs locally, and Fe/Mn oxides are present in the top section. Above 1.38 m lies modern disturbed soil.

4.2.2 Core DJQ

The muddy sediments above 35.85 m in core DJQ were divided into seven units from the base upwards according to lithological changes (Figure 5) and are described as follows.

Unit I (35.85–33.74 m; 9,975–9,810 cal. yr BP) consists of grayish-brown and brownish-gray silty mud (Figure 4L) with locally occurring interbedded silty clay and clayey silt. Plant fragments are common, and pieces of wood are present at the top. There is gradual contact with the overlying unit II.

Unit II (33.74–28.70 m; 9,810–8,620 cal. yr BP) consists of gray, homogeneous mud with a few silt laminations and clumps (Figure 4M). Shell fragments are common. There is gradual contact with the overlying unit III.

Unit III (28.70–19.80 m; 8,620–8,025 cal. yr BP) consists of gray mud with silty clumps and laminations with a thickness of 1–3 mm, which are more obvious upwards (Figure 4N). Bioturbation is evident. There are several shell fragments in the top section. Gradual contact occurs with the overlying unit IV.

In Unit IV (19.80–17.00 m; 8,025–7,615 cal. yr BP), gray homogeneous mud prevails with some silt, mollusk shell fragments, and gastropod shells (Figure 4O). There is gradual contact with the overlying unit V.

Unit V (17.00–13.88 m; 7,615–7,465 cal. yr BP) is composed of a mixture of gray silt and mud (Figure 4P). The mud content increases upwards, and interbedded silt and mud occur locally. Shell fragments are common. Burrows are present in the upper part, which has gradual contact with the overlying unit VI.

Unit VI (13.88–6.45 m; 7,465–7,120 cal. yr BP) is composed of massive silty mud with some silty clumps (Figure 4Q).

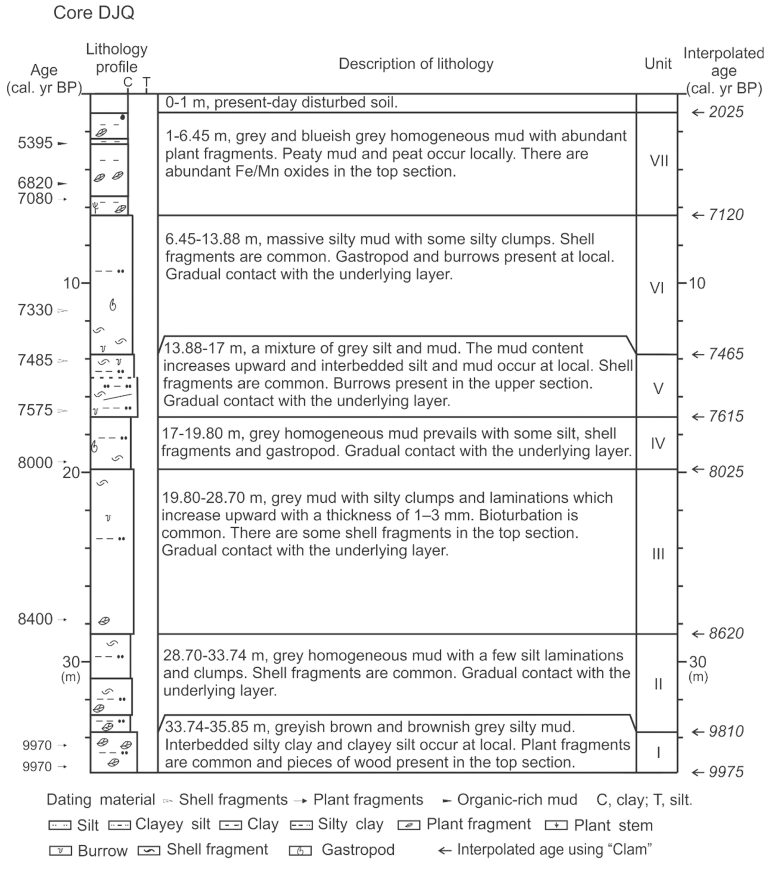

FIGURE 5
Sedimentary profile of core XY, including lithology description and calibrated radiocarbon ages. Interpolated median ages by "Clam" at the boundaries of each unit are indicated on the right.

Mollusk shell fragments are common, and gastropod shells and burrows are locally present. There is gradual contact with overlying unit VII.

Unit VII (6.45–1.00 m; 7,120–2,025 cal. yr BP) consists of gray and blueish-gray homogeneous mud with abundant plant fragments (Figure 4R). Peaty mud and peat are evident locally. There are abundant Fe/Mn oxides in the top section. Modern disturbed soil occurs above 1.00 m.

4.3 Grain size variations in core XY

The grain size in XY varies consistently with lithological units (Figure 3) and is described as follows.

Sediments of unit I (11,125–10,525 cal. yr BP) are mainly composed of silt and clay, which account for 67.6% and 28.2%, respectively. The median grain size (Md) varies from 5.6 to 23.2 μm with a mean value of 12.1 μm. The peak grain size frequency (i.e., the brightest band in Figure 3) in this unit is 32–40 μm.

In unit II (10,525–9,940 cal. yr BP), clay content increases slightly to 29.7%, while silt content decreases to 66.0%. Accordingly, Md decreases to 4.2–36.5 μm, with a mean value of 10.5 μm and the most frequent grain size decreases to 5–10 μm.

Clay content declines markedly to 16.2% in unit III (9,940–9,620 cal. yr BP) and silt remains the dominant fraction (69.6%), while sand content increases to 14.2%. Md rises to 23.3–39.1 μm with a mean value of 28.7 μm. The most frequent grain size lies between 32 μm and 63 μm.

In unit IV (9,620–8,815 cal. yr BP), clay increases substantially to 31.4%, while silt decreases to 65.0%. Md is lower (6.5–28.1 μm), with a mean value of 8.6 μm. The most frequent grain size is much reduced (8–16 μm).

Sediments in unit V (8,815–8,340 cal. yr BP) consists mainly of silt and clay, which account for 67.8% and 20.3%, respectively. Md ranges from 11.3 μm to 32.5 μm with a mean value of 18.2 μm. The peak grain size frequency is 32–63 μm.

In unit VI (8,340–7,515 cal. yr BP), clay content slightly increases to 25.3%, while silt content decreases to 62.7%. Md decreases to 8.3–28.8 μm with a mean value of 12.8 μm. The frequency peak of grain size shifts from 28–40 μm to 8–10 μm from the bottom upwards.

Both clay (18.8%) and silt (47.4%) contents are markedly lower, while sand reaches its highest levels in the core (33.8%) in unit VII (7,515–7,160 cal. yr BP). The median grain size increases to 13.2–61.8 μm with a mean value of 30.0 μm. The most frequent grain size shifts to 74–125 μm and presents consistently as the brightest band of the core (Figure 3).

In unit VIII (7,160–6,110 cal. yr BP), clay content increases again to 32.0% and silt content is 65.0%. Md decreases to 5.9–10.0 μm with a mean value of 7.4 μm. The most frequent grain size is substantially reduced to 8–16 μm.

Sediments of unit IX (6,110–1,290 cal. yr BP) are composed mainly of silt and clay, which account for 68.9% and 28.5%, respectively. Md is low (7.0–11.8 μm) with a mean value of 8.5 μm. The peak grain size frequency (8–16 μm) is consistent with the underlying unit VIII.

4.4 Foraminiferal distribution in core XY

Among the 130 samples in core XY, 13,968 counts of foraminiferal tests representing 15 genera and 28 species (including the undetermined species) were identified from 103 samples. Based on the previous investigation of alive foraminifera in the surficial sediments of the East China Sea (Wang et al., 1988), all identified species are divided into three groups, including the euryhaline and brackish water taxa (salinity <25‰) which live in the tidal flats, the coastal water taxa (salinity 10–30‰) which live in the inner shelf (water depth <50 m), and the offshore water taxa (salinity ≥31‰) which occupy the middle shelf (water depth 50–100 m; Figure 6). In total, 64 samples contain absolute foraminiferal abundances exceeding 100 counts/20 g dry sample and were used to calculate percentages (i.e., relative abundance). The most abundant species is euryhaline *Ammonia beccarii* vars. with a mean relative abundance of 62%, followed by the brackish water species *Cribronionion porisuturalis* with a mean relative abundance of 10%. Other common taxa (i.e., relative abundance >2%) include the euryhaline and brackish water species *Elphidiella kiangsuensis*, *Elphidium magellanicum*, *Cribronionion subinsertum*, coastal water species *Protelphidium tuberculatum*, *Elphidiella hispidulum*, *Quinqueloculina akneriana rotunda*, *Ammonia annectens*, *Elphidium advenum*, *Florilus decorus*, *Elphidium asiaticum*, and offshore water species *Ammonia compressiuscula*.

The absolute abundances of foraminifera in lithological units I–III and IX are mostly lower than 100 counts/20 g and they are therefore not described individually. The main species across these units is *A. beccarii* vars. (Figure 6). Units IV–VIII exhibit higher foraminiferal abundances and the variations in the assemblage are basically consistent with the lithological units. Vertical foraminiferal distributions are therefore described according to lithological units as follows (Figure 6).

Unit IV (33.20–25.55 m; 9,620–8,815 cal. yr BP). Absolute abundance of individuals here is 220 counts/20 g and simple diversity (number of species) is 12. A. *beccarii* vars. has the highest relative abundance (67%), followed by *C. porisuturalis* (22%). Other common species include the brackish water *E. kiangsuensis* (5%) and coastal water *E. hispidulum* (3%) and *P. tuberculatum* (2%). Euryhaline and brackish water taxa account for the vast majority (95%), while coastal water taxa only account for 5%.

Unit V (25.55–21.00 m; 8,815–8,340 cal. yr BP). Absolute abundance decreases to 180 counts/20 g and simple diversity increases to 16. The relative abundance of *A. beccarii* vars. decreases sharply to 38%, while the coastal water species *P. tuberculatum* increases to 30%. Other common species are *C. porisuturalis* (10%), *E. kiangsuensis* (14%), and *E. hispidulum*

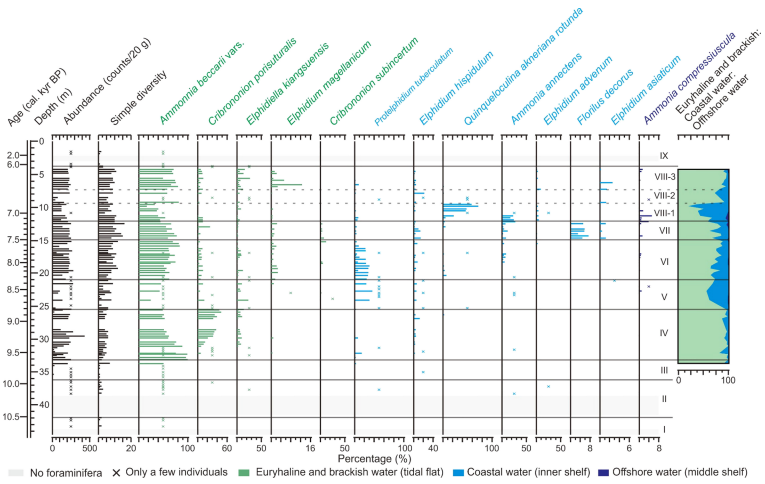

FIGURE 6
Vertical distribution of absolute abundance, simple diversity, and relative abundances of major foraminiferal species in core XY. The ratios of euryhaline and brackish water species, coastal water species, and offshore water species are also indicated.

(6%). Euryhaline and brackish water taxa decrease to 62%, while coastal water taxa markedly increase to 37%.

Unit VI (21.00–14.95 m; 8,340–7,515 cal. yr BP). Absolute abundance increases again to 220 counts/20 g and simple diversity rises to 18. A. *beccarii* vars. returns to being the most abundant taxa (65%), while *P. tuberculatum* decreases to 16%. Other common species are *C. porisuturalis* (5%), *E. kiangsuensis* (4%), *E. hispidulum* (3%), and *A. annectens* (2%). Euryhaline and brackish water taxa account for the substantial majority (76%), while coastal water taxa decrease to 23%.

Unit VII (14.95–12.12 m; 7,515–7,160 cal. yr BP). Absolute abundance decreases slightly to 200 counts/20 g and simple diversity increases further to 24. This unit remains dominated by *A. beccarii* vars. (63%), although there are clear increases in the abundance of coastal and offshore water species including *A. annectens* (8%), *F. decorus* (4%), and *A. compressiuscula* (1%) which occupy the inner and middle shelf regions of the East China Sea (Wang et al., 1988). Other common species include *C. porisuturalis* (6%), *C. subinsertum* (3%), *E. kiangsuensis* (2%), *E. hispidulum* (7%), *P. tuberculatum* (2%), and *Q. akneriana rotunda* (1%). Euryhaline and brackish water taxa account for 74%, while coastal water taxa account for 24%.

Unit VIII (12.12–3.78 m; 7,160–6,110 cal. yr BP). Three subunits can be identified according to variations in foraminiferal assemblages. In subunit VIII-1 (12.12–9.55 m; 7,160–6,835 cal. yr BP), absolute abundance decreases markedly to 140 counts/20 g, and simple diversity is 15. Coastal water species *Q. akneriana rotunda* are especially common (36%), while the relative abundance of *A. beccarii* vars. decreases sharply to 38%. Other common species include *A. annectens* (9%), *P. tuberculatum* (3%), *E. kiangsuensis* (3%), *C. porisuturalis* (3%), *E. advenum* (3%), *E. hispidulum* (1%), and *A. compressiuscula* (1%). Euryhaline and brackish water taxa decrease significantly to 45%, while coastal water taxa increase to 52%, and the remainder (just 3% of them) are offshore water taxa.

Absolute abundance increases to 200 counts/20 g and simple diversity is 12 in subunit VIII-2 (9.55–7.85 m; 6,835–6,620 cal. yr BP). *A. beccarii* vars. becomes dominant (70%) again, followed by 14% of *E. hispidulum*. Other common species include *C. porisuturalis* (6%), *E. kiangsuensis* (6%), *P. tuberculatum* (1%), *Q. akneriana rotunda* (1%), and *E. asiaticum* (1%). Euryhaline and brackish water taxa increase markedly to 81%, while coastal water taxa decrease to 17%. In subunit VIII-3 (7.85–3.78 m; 6,620–6,110 cal. yr BP), absolute abundance is 220 counts/20 g and simple diversity is 17. Dominant species are euryhaline and brackish water taxa, of which *A. beccarii* vars. accounts for 68%, *E. kiangsuensis* 11%, *C. porisuturalis* 7%, and *E. magellanicum* 3%. Coastal water species are down to only 9%, including *E. hispidulum* (3%), *E. advenum* (2%), *P. tuberculatum* (1%), and *E. asiaticum* (1%).

5 Discussion

5.1 Evolution of sedimentary environments in the palaeo-Ningbo Bay

Consistent sediment sequences over the past 10,000 years are observed in the two cores, although the timings of sedimentary facies evolution do not always coincide (Figure 7), possibly induced by the different locations of the two cores (Figures 1B, C). According to the lithology, grain size, and foraminiferal characteristics in core XY, together with the lithology in core

DJQ, five phases (A–E) of sedimentary evolution in the palaeo-Ningbo Bay can be inferred as follows (Figures 7, 8).

Phase A (units I–III, 11,125–9,620 cal. yr BP in core XY and unit I, 9,975–9,810 cal. yr BP in core DJQ). The low abundance of foraminifera and the dominance of *A. beccarii* vars. (Figure 6) in units I–III in XY reflect a weak marine influence. Together with the lithological and sedimentological characteristics in both cores, including coarse grain size and the occurrence of abundant plant fragments, we interpret that these units have been formed in a supratidal flat and/or coastal marsh environment (Figures 3, 5, 7). Therefore, we suggest that this phase represents the initial stage of seawater influence through the palaeo-incised valley (Figure 8A).

Phase B (units IV–V, 9,620–8,340 cal. yr BP in core XY, and units II–III, 9,810–8,025 cal. yr BP in core DJQ). The fine sediments in units IV of XY (9,620–8,815 cal. yr BP) and II of DJQ (9,810–8,610 cal. yr BP) and the prevalence of euryhaline and brackish water foraminiferal species (Figure 7) reflect a muddy intertidal environment with low salinity and weak hydrodynamic forces in the palaeo-Ningbo Bay as seawater was confined within the palaeo-incised valleys at that time (Figure 8B). The abrupt coarsening of grain size at 8,815 cal. yr BP in XY and at 8,610 cal. yr BP in DJQ, together with the significant increase in the coastal water species *P. tuberculatum* indicative of the inner shelf (Wang et al., 1988) after 8,815 cal. yr BP in XY reflects a strengthening of hydrodynamic forces accompanying the intrusion of seawater into the bay. We thus suggest an increase in water depth in the palaeo-bay around 8.8–8.6 cal. kyr BP and a retrogradation sequence from intertidal to subtidal deposits at the sites of both cores (Figure 7). Moreover, it is very likely that the previously subaerially exposed terrace between the two palaeo-incised valleys was drowned by sea water owing to the increase in water depth and tidal energy that eventuated a wider palaeo-Ningbo Bay after 8.6 cal. kyr BP (Figure 8C).

Phase C (unit VI, 8,340–7,515 cal. yr BP in XY, and unit IV, 8,025–7,615 cal. yr BP in DJQ). The observation of sediment fining upwards after ca. 8.3–8.0 cal. kyr BP in the two cores

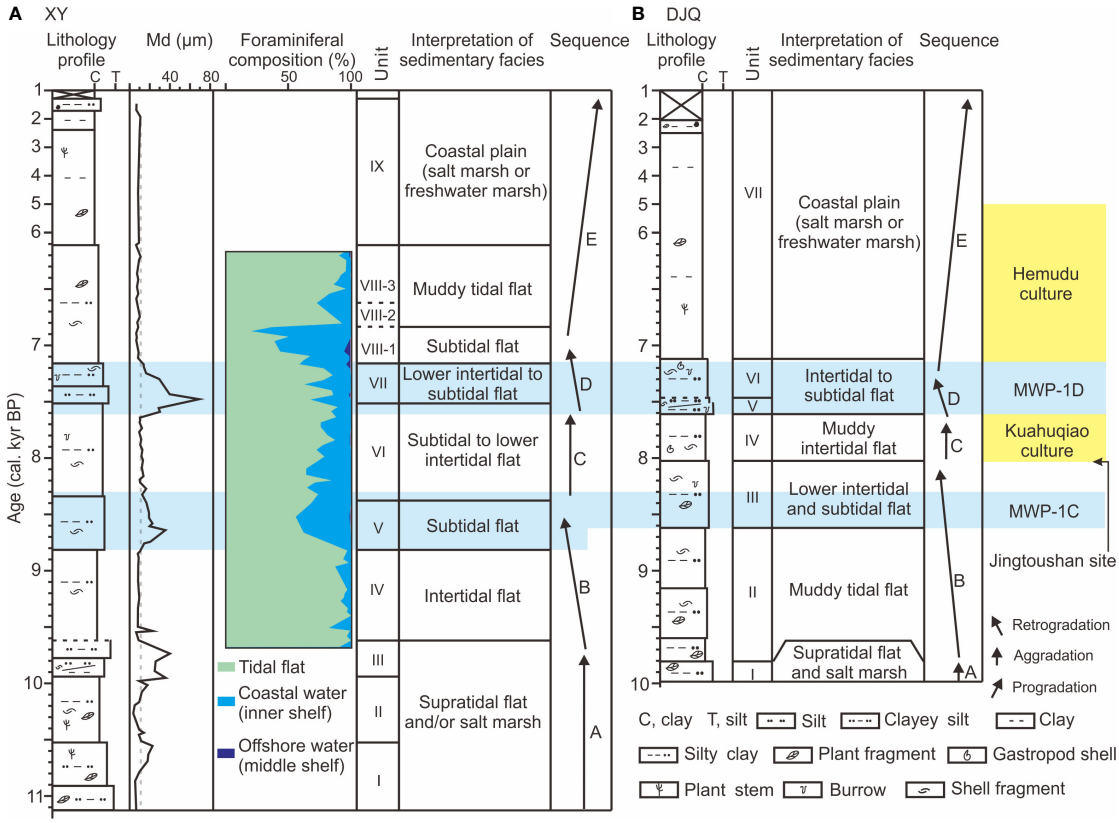

FIGURE 7
Comparison of temporal changes in lithology, grain size, foraminifera, and sedimentary facies, and interpretation of sequences between cores XY **(A)** and DJQ **(B)**. Also indicated are two major periods of strengthened transgression induced by the MWP-1C and MWP-1D events. Impact of MWP-1C commenced later at core site DJQ because of its more inland and sheltered location (Figures 1B, C). The Neolithic Kuahuqiao and Hemudu cultures developed during the periods of relative stable sea levels and the Neolithic Jingtoushan site of shell middens emerged at ca. 8 cal. kyr BP when aggradation of tidal flat dominated in both cores.

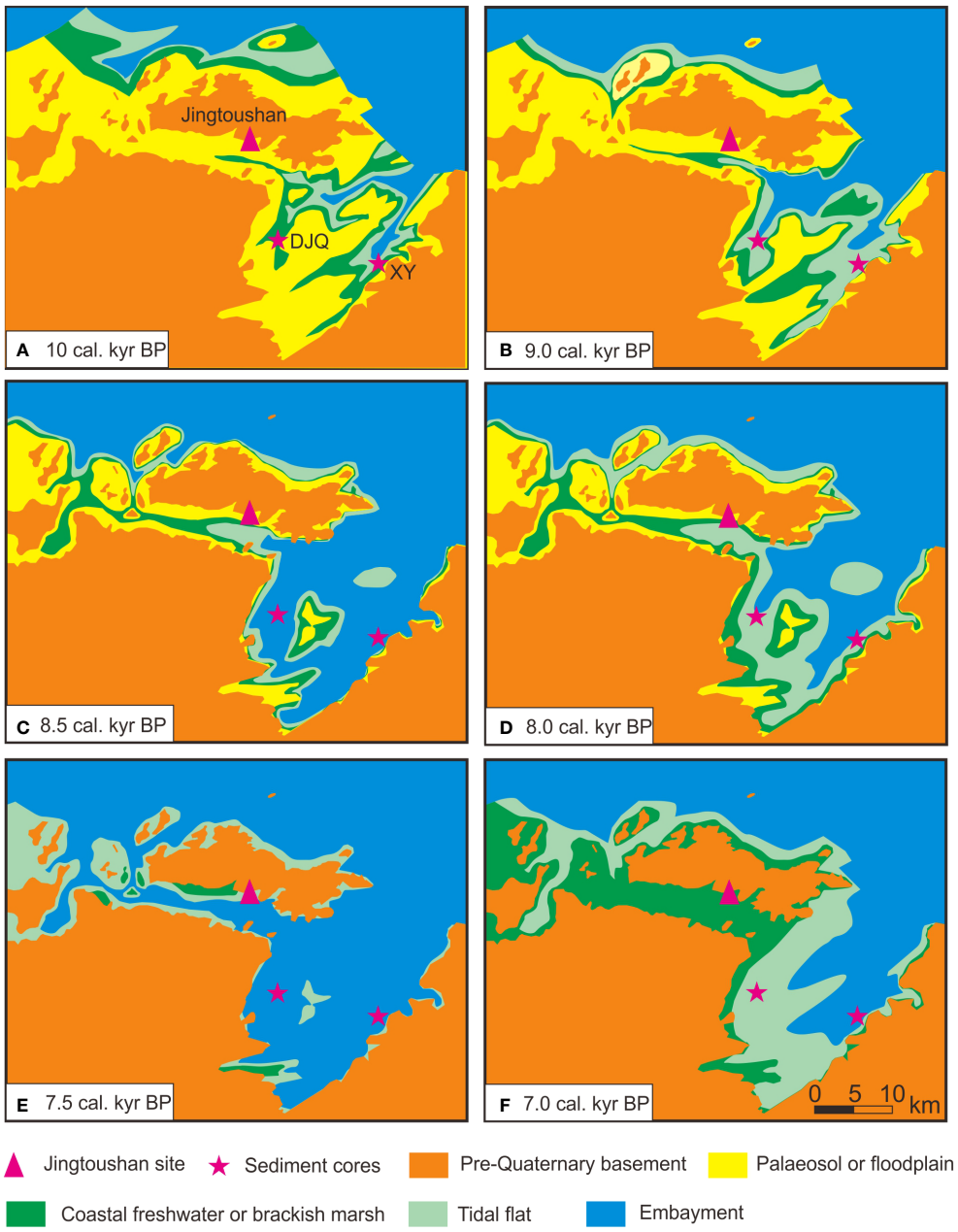

FIGURE 8
Holocene environmental evolution in the Yaojiang Valley and Ningbo Plain **(A–F)** (after Xu, 1987; Yan, 1987; Lyu et al., 2021).

(Figure 7), together with the relatively increasing percentages of euryhaline and brackish water foraminiferal species such as *A. beccarii* vars. in unit VI of XY (8,340–7,515 cal. yr BP; Figure 6), are consistent with aggradation of tidal flat at the core sites. We, therefore, propose that an intertidal flat environment widely developed in the palaeo-bay at ca. 8.0 cal. kyr BP (Figure 8D).

Phase D (unit VII and subunit VIII-1, 7,515–6,835 cal. yr BP in XY, and units V–VI, 7,615–7,120 cal. yr BP in DJQ). Rapid coarsening of grain size is evident at ca. 7.6 cal. kyr BP in both cores, followed by a fining upward succession in core XY during 7.5–6.8 cal. kyr BP (Figures 3, 5). Together with the marked increase in foraminiferal species indicative of the inner and middle shelves (Figure 6), a retrogradation sequence from intertidal flat to subtidal flat can be inferred from unit VII to subunit VIII-1 in XY and in units V and VI in DJQ (Figure 7). The palaeo-Ningbo Bay was therefore possibly fully inundated by seawater at that time (Figure 8E). Previous studies reported

that the palaeo-Yaojiang embayment, located west of the palaeo-Ningbo Bay opened to Hangzhou Bay at ca. 7.6 cal. kyr BP (Lyu et al., 2021), which should also have contributed to the increased tidal energy and strengthened transgression in the palaeo-bay. Moreover, we suggest that this transgression was accompanied by frequent storm events because there is a clear increase in the relative abundance of *A. annectens* and *A. compressiuscula* (Figure 6). High percentages of these two species are often used to identify storm deposits on the coast of Hangzhou Bay because the large, robust, and thick tests of these two species only enrich in the sandy deposits and are indicative of the high energy of storm waves, similar to the coarse-grained sediments (Yan et al., 1989; Xu, 1997; Wang et al., 2018; Wu et al., 2022).

Phase E (subunit VIII-2 to unit IX, 6,835–1,290 cal. yr BP in XY, and unit VII, 7,120–2,025 cal. yr BP in DJQ). The proportion of coastal water foraminiferal species decreases significantly in subunits VIII-2 and VIII-3 of XY, while brackish water species *E. kiangsuensis*, *E. magellanicum*, and *C. porisuturalis* increase in abundance (Figure 6). Taken together, this evidence reflects that the core location again emerged as tidal mudflats as aggradation continued (Figure 7A). After 6,110 cal. yr BP, the organic-rich nature of the mud, and the scarcity of foraminifera tests are consistent with the occurrence of coastal salt marsh or freshwater marsh at the core location of XY (Figures 3, 6). At the more inland site of core DJQ, the aggradational sequence from tidal flat to coastal marsh possibly started at an earlier stage of ca. 7,120 cal. yr BP (Figures 7B, 8F).

5.2 Implications for sea-level change and Neolithic settlement

The sedimentary history of the palaeo-Ningbo Bay outlined above reflects early to mid-Holocene relative sea-level change. Stratigraphic records of both cores indicate strengthened transgression at ca. 8.8–8.6 cal. kyr BP (Figure 7), corresponding to the MWP event, which denotes the accelerated sea-level rise that occurred globally ahead of the marked cooling at 8.2 ka (Barber et al., 1999; Bird et al., 2007; Hijma and Cohen, 2010; Li et al., 2012; Wang et al., 2012; Tjallingii et al., 2014). Previous studies have suggested that this phase of accelerated sea-level rise was associated with the discharge of meltwater and subsequent drainage of the Laurentide proglacial Lakes Agassiz and Ojibway, which occurred at about 8.5–8.3 cal. kyr BP (Hijma and Cohen, 2010; Walker et al., 2012; Harrison et al., 2019). The stratigraphic records in this study reveal that the acceleration of sea-level rise commenced by ca. 8.8 cal. kyr BP, suggesting that a period of climate warming may have prompted the accumulation of meltwater that preceded discharge from the ice-dammed lakes. We suggest that this event can be termed MWP-1C (Figure 7) in the sequence of postglacial MWPs since this event has been claimed to have occurred globally (Harrison et al., 2019).

The tidal flats' aggradational sequence at ca. 8.3 cal. kyr BP in core XY and ca. 8.0 cal. kyr BP in core DJQ most likely occurred in response to the deceleration of sea-level rise at that time (Wang et al., 2013). A retrogradation sequence, resuming at ca. 7.6 cal. kyr BP, is evident in both cores (Figure 7) and reflects renewed marine incursion induced by an event of accelerated sea-level rise at that time, which has been widely described (Blanchon et al., 2002; Bratton et al., 2003; Liu et al., 2004; Behre, 2007; Bird et al., 2007; Yu et al., 2007). Previous studies have reported that sea level records in far-field locations such as the East China coast may reflect eustatic sea-level changes (Clark and Lingle, 1977), and we, therefore, propose that the phase of rapid sea-level rise commencing at ca. 7.6 cal. kyr BP in this study is related to MWP-1D (Figure 7). Meanwhile, progradation from tidal flats to a coastal plain after ca. 7.0 cal. kyr BP developed (Figure 8F) in response to the stabilization of global sea levels at that time (Bard et al., 1996; Lambeck et al., 2014), which halted the creation of new accommodation space in the palaeo-Ningbo Bay.

Moreover, these substantial fundamental early to middle Holocene environmental changes in the palaeo-Ningbo Bay have important implications for ancient human societies along the East China coast (He et al., 2020a; He et al., 2020b; Long, 2022). For example, the settlement at the Neolithic Jingtoushan site at ca. 8.0 cal. kyr BP (Sun et al., 2021) is clearly related to the deceleration of sea-level rise (Wang et al., 2013) and the associated aggradation of tidal mudflats in the bay at that time (Figures 7, 8D). Against this background, the stable shoreline and muddy tidal flats were well suited to the exploitation of reliable marine resources, including shellfish, and facilitated the settlement of Neolithic people, whose activities led to the accumulation of huge shell middens at the Jingtoushan site (Sun et al., 2021). The Kuahuqiao Culture also emerged at ca. 8.0 cal. kyr BP, and rice cultivation even developed in the coastal plain at the head of Hangzhou Bay (ZPICRA (Zhejiang Institute of Cultural Relics and Archaeology) and Xiaoshan Museum, 2004; Zong et al., 2007). However, this study, as evidenced by the foraminiferal assemblage in core XY (Figure 6), reveals that a rapid sea-level rise, contemporaneous with the MWP-1D event at ca. 7.6 cal. kyr BP, provoked marine incursion into the palaeo-bay during ca. 7.5–7.1 cal. kyr BP (Figure 8E). The observation that this rapid transgression was also accompanied by an increased frequency of storm events counters the suggestion by Liu et al. (2018) of weakened marine influence after 7.6 cal. kyr BP. Rather, the flooded bay pounded by extreme storms proved unfavorable to Neolithic settlement and actually precipitated the termination of the Kuahuqiao Culture at ca. 7.6 cal. kyr BP (Zong et al., 2007). This also explains the absence of Neolithic sites in the palaeo-Ningbo Bay during the centuries

after the termination of the Kuahuqiao Culture (ZPICRA, 2019); in contrast, the progradation after ca. 7.0 cal. kyr BP explains the reoccupation by people of the Hemudu Culture at that time (Figures 7, 8F). Therefore, the Neolithic settlement on the coast of Hangzhou Bay was closely linked to phases of stable sea level and the associated aggradation or progradation of the palaeo-bay coastline.

6 Conclusion

This study presents multi-proxy evidence from two early to middle Holocene sediment sequences obtained from the eastern and western sides of the Ningbo Plain, East China coast. Supported by robust age models based on AMS ^{14}C dating, we outline evidence of lithology, grain size, and foraminifera with the aim of reconstructing the Holocene sedimentary history of palaeo-bay as controlled by sea-level change and exploring its relationship to temporal patterns of Neolithic occupation. The following main conclusions are obtained.

1. The Ningbo Plain was inundated by seawater after ca. 9.8 cal. kyr BP, contemporaneously with recorded global sea-level rise. A muddy intertidal to subtidal environment prevailed in the palaeo-bay during the early to mid-Holocene, following which the coastal plain formed after ca. 7 cal. kyr BP as global sea levels stabilized.
2. Evidence of markedly coarse sediments and an increase in the foraminiferal species of coastal waters indicates two periods of submergence of the tidal flats in response to accelerated sea-level rise at ca. 8.8 and 7.6 cal. kyr BP, which likely corresponds to the MWP-1C and MWP-1D events, respectively.
3. Neolithic settlement in the palaeo-Ningbo Bay at ca. 8,000 years ago was facilitated by the aggradation of tidal flats in the palaeo-bay against the background of decelerated or stabilized sea levels at that time. The marine incursion and associated frequent storm events linked to the rapid sea-level rise event of MWP-1D explain the absence of Neolithic occupation in the palaeo-bay after 7.6 cal. kyr BP. The Neolithic settlement was possible again only after ca. 7 cal. kyr BP when the coastal plain became more fully developed.

Data availability statement

The datasets presented in this study can be found in online repositories. The names of the repository/repositories and accession number(s) can be found below: https://data.mendeley.com/datasets/s8tfpv7f62/1.

Author contributions

YL and HX did the field and laboratory work. ZW designed the project and did the field work. YL, MM, and ZW wrote the manuscript. All authors contributed to the article and approved the submitted version.

Funding

This study is supported by the Key R&D Program of Zhejiang Province, China (Grant No. 2022C03141) and the National Key R&D Program of China (Grant No. 2020YFC1521605).

Conflict of interest

The authors declare that the research was conducted in the absence of any commercial or financial relationships that could be construed as a potential conflict of interest.

Publisher's note

References

Barber, D. C., Dyke, A., Hillaire-Marcel, C., Jennings, A. E., Andrews, J. T., Kerwin, M. W., et al. (1999). Forcing of the cold event of 8,200 years ago by catastrophic drainage of laurentide lakes. *Nature* 400 (6742), 344–348. doi: 10.1038/22504

Bard, E., Hamelin, B., Arnold, M., Montaggioni, L., Cabioch, G., Faure, G., et al. (1996). Deglacial sea-level record from Tahiti corals and the timing of global meltwater discharge. *Nature* 382 (6588), 241–244. doi: 10.1038/382241a0

Behre, K. E. (2007). A new Holocene sea-level curve for the southern north Sea. *Boreas* 36 (1), 82–102. doi: 10.1111/j.1502-3885.2007.tb01183.x

Benassai, G., Paola, G. D., and Aucelli, P. P. C. (2015). Coastal risk assessment of a micro-tidal littoral plain in response to sea level rise. *Ocean Coast. Manage.* 104, 22–35. doi: 10.1016/j.ocecoaman.2014.11.015

Bird, M. I., Fifield, L. K., Teh, T. S., Chang, C. H., Shirlaw, N., and Lambeck, K. (2007). An inflection in the rate of early mid-Holocene eustatic sea-level rise: A new

sea-level curve from Singapore. *Estuarine Coast. Shelf Sci.* 71 (3–4), 523–536. doi: 10.1016/j.ecss.2006.07.004

Bird, M. I., Austin, W. E. N., Wurster, C. M., Fifield, L. K., Mojtahid, M., and Sargeant, C. (2010). Punctuated eustatic sea-level rise in the early mid-Holocene. *Geology* 38(9), 803–806. doi: 10.1130/G31066.1

Blaauw, M. (2010). Methods and code for 'classical' age-modelling of radiocarbon sequences. *Quaternary Geochronology* 5, 512–518. doi: 10.1016/j.quageo.2010.01.002

Blanchon, P., Brian, J., Derek, C., and Ford, C. (2002). Discovery of a submerged relic reef and shoreline off grand Cayman: further support for an early Holocene jump in sea level. *Sedimentary Geology* 147 (3–4), 253–270. doi: 10.1016/S0037-0738(01)00143-9

Blanchon, P., and Shaw, J. (1995). Reef drowning during the last deglaciation: Evidence for catastrophic sea–level rise and ice-sheet collapse. *Geology* 23 (1), 4–8. doi: 10.1130/0091-7613(1995)023<0004:RDDTLD>2.3.CO;2

Bratton, J. F., Colman, S. M., Thieler, E. R., and Seal, R. R. (2003). Birth of the modern Chesapeake bay estuary between 7.4 and 8.2 ka and implications for global sea-level rise. *Geo-Marine Lett.* 22 (4), 188–197. doi: 10.1007/s00367-002-0112-z

Clark, J. A., and Lingle, C. S. (1977). Future sea level changes due to West Antarctic fluctuations. *Nature* 269, 206–209. doi: 10.1038/269206a0

Harrison, S., Smith, D. E., and Glasser, N. F. (2019). Late quaternary meltwater pulses and sea level change. *J. Quaternary Sci.* 34 (1), 1–15. doi: 10.1002/jqs.3070

He, K., Lu, H., Li, Y., Ding, F., Zhang, J., and Wang, C. (2020b). Cultural response to middle Holocene sea-level fluctuations in eastern China: a multi-proxy approach. *Boreas* 49, 71–88. doi: 10.1111/bor.12421

He, K., Lu, H., Zheng, H., Yang, Q., Sun, G., Zheng, Y., et al. (2020a). Role of dynamic environmental change in sustaining the protracted process of rice domestication in the lower Yangtze river. *Quaternary Sci. Rev.* 242, 106456. doi: 10.1016/j.quascirev.2020.106456

Hijma, M. P., and Cohen, K. M. (2010). Timing and magnitude of the sea-level jump preluding the 8200 yr event. *Geology* 38 (3), 275–278. doi: 10.1130/G30439.1

Huang, H., Hu, B., Ding, Y., Gu, S., and Zhao, W. (2013). *Research on the planning technology of meteorological disaster prevention in ningbo* (Ningbo: Ningbo Publishing House).

Huang, J., Li, Y., Ding, F., Zheng, T., Meadows, M. E., and Wang, Z. (2021). Sedimentary records of mid-Holocene coastal flooding at a Neolithic site on the southeast plain of Hangzhou Bay, east China. *Marine Geology* 431, 106380. doi: 10.1016/j.margeo.2020.106380

Huang, J., Lei, S., Tang, L., Wang, A., and Wang, Z. (2020). Mid-Holocene environmental change and human response at the Neolithic Wuguishan site in the Ningbo coastal lowland of East China. *The Holocene* 30, 1591–1605. doi: 10.1177/0959683620941070

Innes, J. B., Zong, Y., Chen, Z., Chen, C., Wang, Z., and Wang, H. (2009). Environmental history, palaeoecology and human activity at the early neolithic forager/cultivator site at kuahuqiao, hangzhou, eastern China. *Quaternary Sci. Rev.* 28 (23–24), 2277–2294. doi: 10.1016/j.quascirev.2009.04.010

IPCC (2019). *Special report on the ocean and cryosphere in a changing climate, special report* (Monaco: IPCC). Available at: https://www.ipcc.ch/srocc.

Lambeck, K., Rouby, H., Purcell, A., Sun, Y. Y., and Sambridge, M. (2014). Sea Level and global ice volumes from the last glacial maximum to the Holocene. *Proc. Natl. Acad. Sci. United States America.* 111 (43), 15296–15303. doi: 10.1073/pnas.1411762111

Lamb, A. L., Wilson, G. P., and Leng, M. J. (2006). A review of coastal palaeoclimate and relative sea-level reconstructions using $\delta^{13}C$ and C/N ratios in organic material. *Ear Sci. Rev.* 75 (1), 29–57. doi: 10.1016/j.earscirev.2005.10.003

Li, Y., Tornqvist, T. E., Nevitt, J. M., and Kohl, B. (2012). Synchronizing a sea-level jump, final lake agassiz drainage, and abrupt cooling 8200 years ago. *Earth Planetary Sci. Lett.* 315–316, 0–50. doi: 10.1016/j.epsl.2011.05.034

Liu, Y., Deng, L., He, J., Jiang, R., Fan, D., Jiang, X., et al. (2020). Early to middle Holocene rice cultivation in response to coastal environmental transitions along the south hangzhou bay of eastern China. *Palaeogeography Palaeoclimatology Palaeoecol.* 555, 109872. doi: 10.1016/j.palaeo.2020.109872

Liu, J., Milliman, J. D., Gao, S., and Cheng, P. (2004). Holocene Development of the yellow river subaqueous delta, north yellow Sea. *Mar. Geology* 209, 45–67. doi: 10.1016/j.margeo.2004.06.009

Liu, Y., Sun, Q., Fan, D., Dai, B., Ma, F., Xu, L., et al. (2018). Early to middle Holocene Sea level fluctuation, coastal progradation and the neolithic occupation in the yaojiang valley of southern hangzhou bay, Eastern China. *Quaternary Sci. Rev.* 189, 91–104. doi: 10.1016/j.quascirev.2018.04.010

Long, T. (2022). Contrasting developments of the cultural complexes south and north of hangzhou bay, eastern China, controlled by coastal environmental changes. *Quaternary Int.* 623, 94–100. doi: 10.1016/j.quaint.2021.10.014

Lyu, Y., Tong, C., Saito, Y., Meadows, M. E., and Wang, Z. (2021). Early to mid-Holocene sedimentary evolution on the southeastern coast of hangzhou bay, East China, in response to sea-level change. *Mar. Geology* 442, 106655. doi: 10.1016/j.margeo.2021.106655

McConnaughey, T. A., and Gillilin, D. P. (2008). Carbon isotopes in mollusk shell carbonates. *Geo-Marine Lett.* 28, 287–299. doi: 10.1007/s00367-008-0116-4

Ningbo Water Conservation Annals Compilation Committee (2006). *Ningbo water conservation* (Beijing: Zhonghua Book Company).

Stuiver, M., Reimer, P. J., and Reimer, R. W. (2022) *Calib 8.20*. Available at: http://calib.org/calib/.

Sun, K. (2013). *Research of engineering geology zoning in yao river and fenghua river basin* (Nanjing:: Nanjing University). Master's thesis.

Sun, G., Mei, S., Lu, X., Wang, Y., Zheng, F., and Huang, W. (2021). Jingtoushan neolithic site in yuyao, Zhejiang. *Archaeology* 7, 723–746.

Tang, L. (2020). *Middle Holocene seawater intrusion and human's rapid response in the yaojiang-ningbo coastal plain, East China* (Shanghai: East China Normal University).

Tang, L., Shu, J., Chen, J., and Wang, Z. (2019). Mid- to late Holocene vegetation change recorded at a Neolithic site in the Yangtze coastal plain, east China. *Quaternary International*. 519, 122–130. doi: 10.1016/j.quaint.2018.12.031

Tjallingii, R., Stattegger, K., Stocchi, P., Saito, Y., and Wetzel, A. (2014). Rapid flooding of the southern Vietnam shelf during the early to mid-Holocene. *J. Quaternary Sci.* 29 (6), 581–588. doi: 10.1002/jqs.2731

Walker, M. J. C., Berkelhammer, M., Björck, S., Cwynar, L. C., Long, A. J., Lowe, J. J., et al. (2012). Formal subdivision of the Holocene Series/Epoch: a discussion paper by a working group of INTIMATE (Integration of ice-core, marine and terrestrial records) and the subcommission on quaternary stratigraphy (International commission on stratigraphy). *J. Quaternary Sci.* 27 (7), 649–659. doi: 10.1002/jqs.2565

Wang, Z., Ryves, D. B., Lei, S., Nian, X., Lv, Y., Tang, L., et al. (2018). Middle Holocene marine flooding and human response in the south Yangtze coastal plain, East China. *Quaternary Sci. Rev.* 187, 80–93. doi: 10.1016/j.quascirev.2018.03.001

Wang, J., Yi, S., Li, M., Wang, L., and Song, C. (2017). Effects of sea level rise, land subsidence, bathymetric change and typhoon tracks on storm flooding in the coastal areas of shanghai. *Sci. Total Environ.* 621, 228–234. doi: 10.1016/j.scitotenv.2017.11.224

Wang, P., Zhang, J., Zhao, H., Min, Q., Bian, Y., Zheng, L., et al. (1988). *Foraminifera and ostracoda in bottom sediments of the East China Sea* (Beijing: Ocean Press).

Wang, Z., Zhan, Q., Long, H., Saito, Y., Gao, X., Wu, X., et al. (2013). Early to mid–Holocene rapid sea–level rise and coastal response on the southern Yangtze delta plain, China. *J. Quaternary Sci.* 28, 659–672. doi: 10.1002/jqs.2662

Wang, Z., Zhuang, C., Saito, Y., Chen, J., Zhan, Q., and Wang, X. (2012). Early mid-Holocene sea-level change and coastal environmental response on the southern Yangtze delta plain, China: implications for the rise of neolithic culture. *Quaternary Sci. Rev.* 35, 51–62. doi: 10.1016/j.quascirev.2012.01.005

Woodruff, J. D., Irish, J. L., and Camargo, S. J. (2013). Coastal flooding by tropical cyclones and sea–level rise. *Nature* 504 (7478), 44–52. doi: 10.1038/nature12855

Wu, Y., Huang, X., Zheng, X., Meadows, M. E., and Wang, Z. (2022). Sedimentary records of mid-Holocene extreme storm events on the north bank of Hangzhou Bay, East China. *Marine Geology* 451, 106891. doi: 10.1016/j.margeo.2022.106891

Xiong, H. X., Zong, Y. Q., Li, T. H., Long, T., Huang, G., and Fu, S. (2020). Coastal GIA processes revealed by the early to middle Holocene sea level history of east China. *Quaternary Sci. Rev.* 233, 1–15. doi: 10.1016/j.quascirev.2020.106249

Xu, J. (1987). *Holocene Evolution of shoreline and sedimentary facies in the yuyao-cixi plain on south coast of hangzhou bay* (Shanghai: East China Normal University). Master thesis.

Xu, S. (1997). *Storm deposits in the Yangtze delta* (Beijing: Science Press).

Yan, J. (1987). *Holocene Stratigraphy and sedimentary environmental evolution in ningbo plain* (Shanghai: East China Normal University). Master thesis.

Yan, Q., Xu, S., and Shao, X. (1989). Holocene Cheniers in the Yangtze delta, China. *Mar. Geology* 90 (4), 337–343. doi: 10.1016/0025-3227(89)90135-7

Yoneda, M., Uno, H., Shibata, Y., Suzuki, R., Kumamoto, Y., Yoshida, K., et al. (2007). Radiocarbon marine reservoir ages in the western pacific estimated by pre–

bomb molluscan shells. *Nucl. Instruments Methods Phys. Res. Section B Beam Interact. Materials Atoms* 259 (1), 432–437. doi: 10.1016/j.nimb.2007.01.184

Yu, S., Berglund, B. E., Sandgren, P., and Lambeck, K. (2007). Evidence for a rapid sea-level rise 7600 yr ago. *Geology* 35 (10), 891–894. doi: 10.1130/G23859A.1

Zheng, Y., Sun, G., and Chen, X. (2012). Response of rice cultivation to fluctuating sea level during the Mid-Holocene. *Chinese Science Bulletin* 57, 370–378. doi: 10.1007/S11434-011-4786-3

Zong, Y., Chen, Z., Innes, J. B., Chen, C., Wang, Z., and Wang, H. (2007). Fire and flood management of coastal swamp enabled first rice paddy cultivation in east China. *Nature* 449 (7161), 459–462. doi: 10.1038/nature06135

ZPICRA (Zhejiang Institute of Cultural Relics and Archaeology) and Xiaoshan Museum (2004). *Kuahuqiao* (Beijing: Cultural Relics Press).

ZPICRA (2019). *The archaeology of zhejiang province 1979-2019* (Beijing: Cultural Relics Press).